Plasmonics (2013) 8:1011–1016
DOI 10.1007/s11468-013-9503-4

Slab Thickness Dependence of Localized Surface Plasmon Resonance Behavior in Gold Nanorings

Chia-Yang Tsai · Che-Yao Wu · Kai-Hau Chang · Po-Tsung Lee

Received: 31 October 2012 / Accepted: 30 January 2013 / Published online: 12 February 2013

Abstract We present detailed experimental and numerical studies of plasmonic properties of gold nanoring (NR) arrays with different slab thicknesses from 15 to 125 nm. The hybrid plasmon resonances for the bonding and antibonding modes in gold NRs exhibit a high slab thickness dependence behavior in optical properties. For the thinner slab thickness below 50 nm, both hybrid modes show large spectral tunabilities by varying the slab thickness. Furthermore, for such hollow NR structure, the enhancements of electric field intensities at the inner and outer ring surfaces when reducing the slab thickness are investigated. We observe a significant transition of field distributions for the antibonding mode. All these features can be understood by surface charge distributions from our simulations. The results of this study offer a potential strategy to design a composite plasmonic nanostructure with large field enhancement for numerous applications.

Keywords Surface plasmon · Plasmonic array · Nanoring

Introduction

In recent decades, noble metal nanostructures have been widely studied since they can support localized surface plasmon resonances (LSPR) which exhibit enhanced optical fields surrounding metal nanoparticles when interacting with incident electromagnetic waves [1]. This unique feature of near-field enhancement effect has been exploited in many fascinating applications including surface-enhanced spectroscopy [2, 3], chemical and biomedical sensing [4, 5], solar energy device [6, 7], and optical nanotrapping [8, 9]. However, the ability to generate high field enhancements is strongly determined by nanoparticle geometry. Thus, plasmonic properties of a train of nanostructure shapes have been explored, such as nanoprisms [10], nanorods [11], nanowells [12], and nanograils [13]. In particular, ring-shaped nanoparticles have attracted great research interest recently since such nanostructures can produce high local fields arisen from strong coupling of inner and outer surface plasmons [14–16]. In addition, they provide an additional electric field in the cavity region of the ring structure, which is particularly beneficial for practical applications that need high volumes of enhanced fields such as sensing application and surface-enhanced spectroscopy. Therefore, in the last few years, many researchers have investigated the improvements of index sensing [17] and surface-enhanced Raman scattering [18] by using gold nanoring (NR) particles due to their superior optical properties.

To explain the optical properties of metal NR, the plasmon hybridization model has been proposed [19, 20], which is also used to describe the plasmon response of other hybrid nanostructures successfully, such as nanoshells [21], nanoeggs [22], nanomatryushkas [23], and nanorices [24]. For the NR structure, the LSPR characteristics can be regarded as the mixing of plasmonic behaviors of two elementary geometries, a nanodisk and a nanohole [25]. This hybridization effect from both nanostructures gives rise to two hybrid plasmonic modes in metal NR, referred to as antibonding (A) and bonding (B) resonance modes, respectively [14, 15].

Interestingly, the optical properties of both hybrid plasmonic modes are very sensitive to the NR geometry, which results from the strong interaction between nanodisk and nanohole plasmons supported by the outer and inner surfaces of metal NR. This indicates that the LSPR in metal NR

C.-Y. Tsai · C.-Y. Wu · K.-H. Chang · P.-T. Lee (✉)
Department of Photonics and Institute of Electro-Optical Engineering, National Chiao Tung University,
Rm. 413 CPT Building, 1001 Ta-Hsueh Road,
Hsinchu 300, Taiwan
e-mail: potsung@mail.nctu.edu.tw

can be easily tuned by the dimension and width of the ring. This high tunability of plasmonic resonances in gold NR by adjusting the ratio of the ring width to its radius has been investigated by Aizpurua et al. [14]. However, the optical behaviors of hybrid plasmonic modes in gold NR when varying the vertical height of the slab have not been studied yet. In this work, we report our experimental and simulation investigations of the A and B modes in gold NRs with different slab thicknesses. Moreover, we focus on the field intensity enhancement at the inner and outer gold NR surfaces as the slab thickness is decreased. This work can advance our understanding of the optical properties of the hybrid modes in a plasmonic hollow structure with varied slab thickness and greatly facilitate our abilities to design the hybrid plasmonic nanostructure.

Fabrication and Measurement

The scheme of a gold NR structure with average ring width w, diameter d, and slab thickness t is shown in Fig. 1a. In our fabrication, commercial indium tin oxide (ITO) glass was utilized as the substrate since such electrically conductive substrate can preclude the charging effect during electron beam lithography (EBL) process. First, the ITO glass substrate was cleaned by ultrasonication in acetone and isopropyl alcohol followed by rinsing with deionized water and blow-drying with nitrogen. Each of the sonication steps was carried out at room temperature for 5 min. The substrate was then spin-coated a 150-nm polymethylmethacrylate (PMMA) layer, and NR array patterns with areas of 300×300 μm^2 were defined on the PMMA layer by the EBL method. After exposure and development, the substrate was deposited with a gold thin film using thermal evaporation. Then, the standard lift-off procedure was accomplished by immersing the sample in acetone for a few hours. Figure 1b shows a selected scanning electron microscope (SEM) image of the fabricated gold NR array with the slab thickness of 50 nm. The average ring width and diameter of fabricated gold NRs are fixed at 160 and 500 nm, respectively. Importantly, the period of gold NR array was set at 1,000 nm which was large enough to reduce the near-field coupling between each gold NR particle. In addition, to confirm the slab thickness of each gold NR array, the morphological features of gold NR arrays were analyzed using atomic force microscopy (AFM). Figure 1c shows a typical 2D AFM micrograph of gold NR array with the slab thickness of 50 nm. We make sure that the slab thicknesses of gold NRs can be well controlled during the metal deposition process.

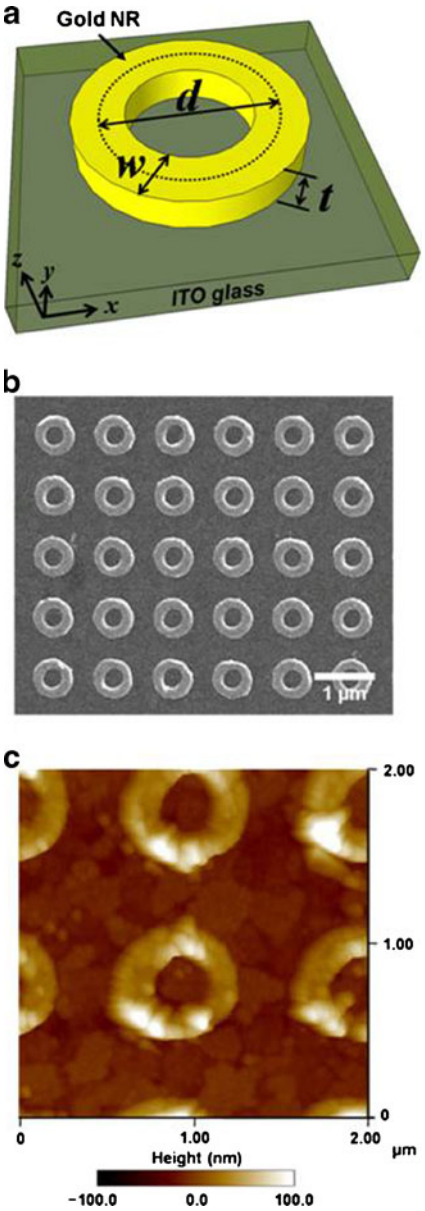

Fig. 1 **a** Schematic diagram of the gold NR structure design. The structural key parameters are defined as w=average ring width, d=diameter, and t=slab thickness. **b** Top view SEM image of the fabricated gold NR array with w=160 nm, d=500 nm, and t=50 nm on ITO glass. The period of plasmonic array is fixed at 1,000 nm. **c** Typical 2D AFM micrograph of the gold NR array with the slab thickness of 50 nm

The optical properties of gold NR arrays with different slab thicknesses were studied using upright transmission spectroscopy which uses a halogen lamp as the light source. Light was focused on gold NR arrays through a ×20 objective lens. To minimize edge effect, a spot size of around 150 μm in diameter on the sample surface sufficiently smaller than the dimension of the fabricated array was attained by using the iris diaphragms and collimating lens. The transmitted light was then collected by another ×20

objective lens and focused on a multimode optical fiber connected to an optical spectrum analyzer. The extinction spectra can be obtained using the following equation:

$$Extinction(\lambda) = -log\frac{I_{out}(\lambda)}{I_{ref}(\lambda)}$$

where $I_{out}(\lambda)$ and $I_{ref}(\lambda)$ are the intensities of the transmitted light with and without the gold NR array.

Results and Discussions

To investigate the influence of thickness on the optical behaviors of the A and B modes in gold NRs, the slab thickness t was varied systematically for a wide range from 15 to 125 nm. Figure 2a shows the measured extinction spectra of gold NR arrays with various slab thicknesses. The gold NR arrays exhibit two well-defined LSPR modes in the visible and near-infrared ranges corresponding to the A and B modes, respectively. Moreover, we observe a blue-shifted shoulder in the B mode around 1,100 nm, which is the grating-induced mode attributed from a periodic array. This phenomenon has been investigated experimentally in the previous work for gold nanoparticle arrays [26]. To further investigate the trends of peak wavelength shifts, the measured peak wavelengths of both A and B modes in gold NRs with different slab thicknesses are plotted in Fig. 2c. For both A and B modes, remarkable redshifts are observed by reducing the slab thickness. This redshift behavior of the LSPR mode with decreasing height of the plasmonic nanostructure has been investigated, such as nanoplate [27], nanohole [28], and nanocrescent [29]. Moreover, we find experimentally that the A modes are shifting more while the B modes are less redshifting, which indicates that the B mode is less sensitive to thickness changes in a periodic array. This result can be ascribed to the grating-induced mode in a periodic array, since the restoring force in gold NR could be strengthened due to the in-phase addition of radiation fields from the grating-induced mode when the grating-induced mode is coupled to the B mode. We would expect the suppression of the redshifting for the B mode. Interestingly, we find that the A mode at around 690 nm does not exhibit any distinguishable shift as the slab thickness is decreased gradually from 125 to 50 nm, which differs from the B mode. The disparity between these two modes is related to plasmonic charge distributions. For the thicker slab thickness, the restoring force of the electric dipole in gold NR is cancelled from the antisymmetric charge distribution of the A mode, which leads to the unvaried plasmon frequency. The analysis of corresponding charge distributions will be discussed in detail later.

To verify the effect of slab thickness on the optical response of gold NRs, the extinction spectra of such plasmonic structure with varied slab thickness were calculated using the 3D finite element method by COMSOL Multiphysics simulation software. We set up the simulated domain for a single gold NR and employed the Lorenz–Drude model for the dielectric function of gold NR. The environmental refractive index was set to be 1.0 for air, and the dispersion of the ITO substrate was considered. Furthermore, the structural dimensions of NRs used in

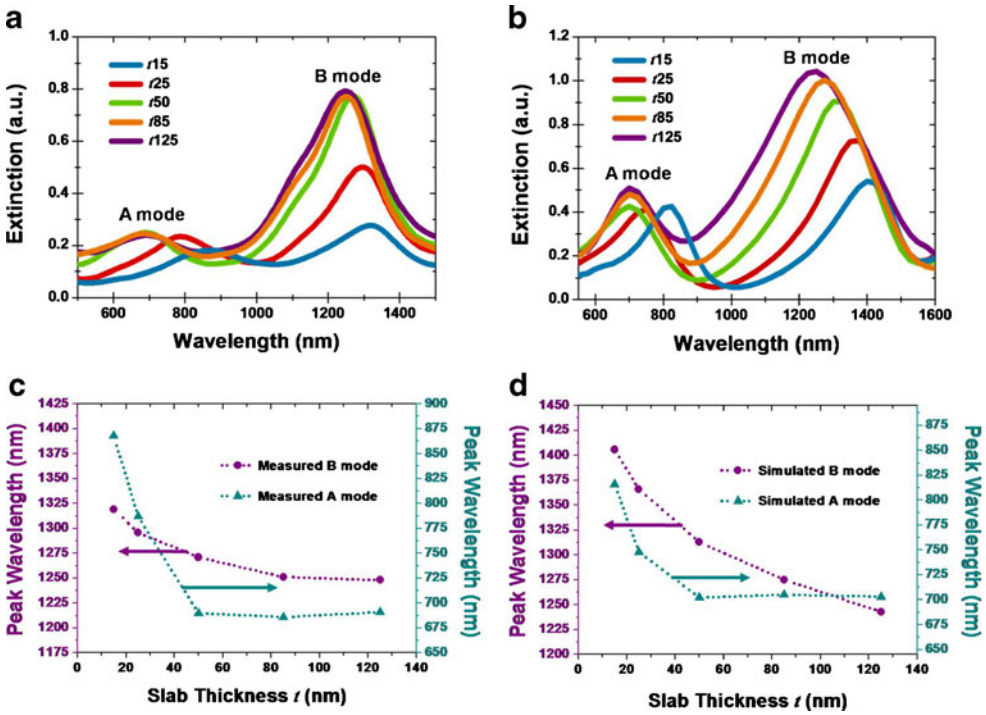

Fig. 2 **a** Measured and **b** simulated extinction spectra of gold NRs with varied slab thickness t within a range of 15–125 nm. **c** Measured and **d** simulated peak wavelengths of the A and B modes in gold NRs with different slab thicknesses t

these simulations were identical to those of fabricated NRs. Panels b and d of Fig. 2 show the simulated extinction spectra and peak wavelengths of gold NRs with the slab thicknesses varied from 15 to 125 nm. It is clear that the computational results are in good agreement with the experimentally observed trends. As the slab thickness decreases, two distinct peaks identified as the A and B modes exhibit apparent redshifts. Particularly, the peak wavelength of the A mode does not shift when the slab thickness is varied within the range of 50 to 125 nm. The feature of such simulated result is clearly reproduced in our experiment. Furthermore, we can see that the line widths of the measured bonding modes are obviously narrower than those of the calculated ones. This is because the grating effect in a periodic array results in the reducing of the line width owing to the coherent interactions of nanostructures [30]. However, in our simulation, the scattering boundary condition for all the external boundaries of the computational domain is used to study the thickness effect without considering any optical couplings.

It is also interesting to study the near-field changes when we vary the slab thickness of gold NR. The field intensity distributions of both A and B modes in the vertical cross sections and horizontal middle planes of gold NRs with different slab thicknesses are shown in Fig. 3a and b, respectively. For the B mode, the electric field distribution at the outer and inner surfaces of gold NR resulting from the symmetric charge pattern [14] is observed. However, the near-field profile of the A mode is obviously dissimilar to that of the B mode. The strong near fields of the A mode are spatially concentrated in the cavity region of the gold NR for the greater slab thickness. As the slab thickness is decreased gradually, an obvious transition in field distribution of the A mode can be clearly seen, which exhibits an apparent enhancement of the electric field at the inner and outer surfaces of gold NR when the slab thickness is less than 50 nm. Such electric field intensity profile of the A mode with the thinner slab thickness is analogous to that of the B mode, which is caused by the symmetric charge pattern on the top surface of the ring due to the redistribution of surface charges.

To understand the intensity enhancement properties of gold NR, we further focus on the electric field intensities of the A and B modes at the inner and outer surfaces of gold NRs with different slab thicknesses, as shown in Fig. 4a and b. For the outer NR surface, the intensity enhancements of around eight and three times for the A and B modes, respectively, are obtained as the slab thickness is decreased from 125 to 15 nm. Furthermore, the field intensity of the B mode is always larger than that of the A mode for gold NR at a certain slab thickness. This phenomenon can be explained by the strong coupling from the symmetric charge distribution at the inner and outer surfaces of the ring for the B mode. For the inner NR surface, the intensity enhancements of around 2.5 and 4 times for the A and B modes are obtained as slab thickness is reduced from 125 to 15 nm. Apparently, whether at the outer or inner surface of the NR, the field intensities exhibit exponential growth with decreasing slab thickness for both A and B modes. This significant intensity enhancement is caused by the enhanced coupling of the electric field at the top and bottom surfaces of gold NR.

In order to comprehend the surface charge distributions of gold NRs, we calculated charge distribution profiles of the

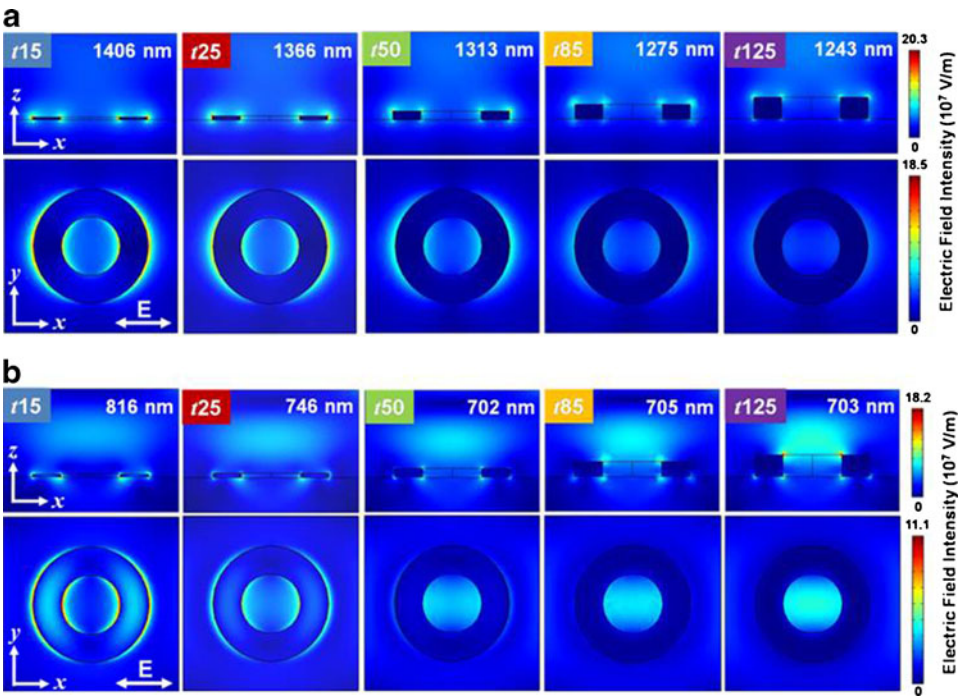

Fig. 3 Electric field intensity distributions of the **a** B and **b** A modes in the cross sections and middle planes of gold NRs with different slab thicknesses

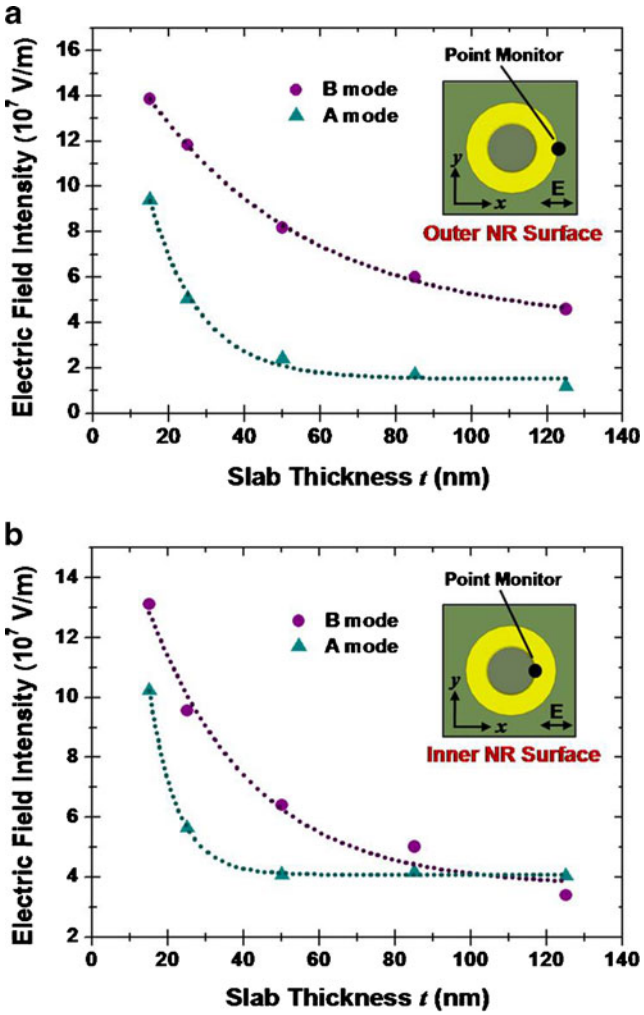

Fig. 4 Electric field intensities of the A and B modes at the **a** outer and **b** inner surfaces (denoted by the *point monitors*) of gold NR as a function of slab thickness. The *dotted lines* show the best fit of these data to the exponential decay function

corresponding resonance modes in gold NRs with slab thicknesses of 125 and 15 nm, as shown in Fig. 5a and b. In Fig. 5a, the charge distribution of the B mode shows the same signs at the inner and outer NR surfaces corresponding to symmetric charge distribution, which exhibits a typical dipole-like charge pattern. Furthermore, the surface charges for the B mode maintain their distribution as the slab thickness is decreased from 125 to 15 nm. Oppositely, the antisymmetric charge distribution of the A mode on the inner and outer NR surfaces for the slab thickness of 125 nm is observed. From the cross-sectional view in Fig. 5b (top), antisymmetric charge distribution corresponding to the reversed dipole moments for the top and bottom NR surfaces is found. This feature of the A mode is in good agreement with the calculation results obtained for silver nanoring [25]. Such antisymmetric distribution of surface charges causes the cancellation of restoring force in gold NR, which results in invariant resonance frequency of the A mode when varying the slab thickness. In particular, the charge distribution of the A mode shows a noticeable transformation as the slab thickness is decreased below 50 nm. The same trend is also observed from the peak wavelength shifts and field intensity distributions. We ascribed this transformation to the charge redistribution resulted from the moving of surface charges. From the charge distribution of the A mode on the top surface for the slab thickness of 125 nm, high charge densities are located at the inner surface of gold NR, as shown in Fig. 5b (top). These high-density surface charges on the inner surface would move to the outer surface when the slab thickness is decreased. Thus, as shown in Fig. 5b (bottom), the charge distribution on the inner surface for the slab thickness of 15 nm exhibits lower density compared with that for the slab thickness of 125 nm, and the redistributed positive and negative charges occupy the two sides of the top surface, respectively, which leads to the symmetric charge distribution on the top surface of NR. This result further elucidates that the mode profile for the A mode

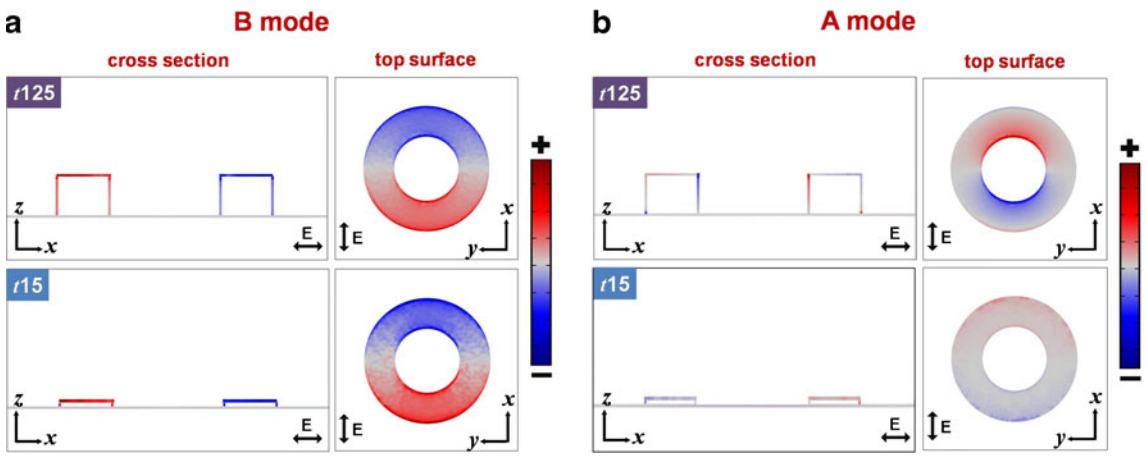

Fig. 5 Charge distribution profiles of the **a** B and **b** A modes in gold NRs with slab thicknesses of 125 nm (*top*) and 15 nm (*bottom*) for the cross-sectional view (*left*) and top surface (*right*)

of gold NR with thinner slab thickness is similar to that of the B mode, which exhibits field enhancements at both inner and outer surfaces.

Conclusion

We study experimentally and numerically the slab thickness effect on the optical behaviors of hybrid plasmonic modes in gold NRs. By changing the slab thickness, both hybrid modes in gold NRs exhibit high spectral tunabilities. From experimental observations, both A and B modes of gold NRs display redshift behavior as the slab thickness is decreased, which is confirmed by our numerical studies. Particularly, the resonance wavelength of the A mode in gold NRs for a greater slab thickness above 50 nm does not show an apparent shift, which is due to the mutual cancellation of dipole force from the antisymmetric charge pattern of the A mode. This feature has been verified by surface charge distribution profiles from numerical calculations. Moreover, the slab thickness dependence of associated electric field intensity is also numerically investigated and discussed, especially on the inner and outer NR surfaces. By reducing the slab thickness, we find that the field intensities of these two hybrid modes at both positions can be improved and also observe an obvious transition in field distribution of the A mode due to the redistribution of surface charges. These results further advance our understanding of the characteristics of hybrid plasmonic structures with varied vertical slab thickness and render a useful design principle to fabricate such nanoparticles with a highly enhanced field for practical applications that require large localized field enhancement, such as nanolasing, plasmonic-based sensors for chemical and biomedical applications, surface-enhanced spectroscopy, and nanoparticle trapping.

Acknowledgments This work is supported by Taiwan's National Science Council (NSC) under contract nos. NSC-101-2221-E-009-054-MY2 and NSC-100-2221-E-009-109-MY3. The authors would like to thank the Center for Nano Science and Technology (CNST) at National Chiao Tung University (NCTU), Taiwan, for the help.

References

1. Barnes WL, Dereux A, Ebbesen TW (2003) Surface plasmon subwavelength optics. Nature 424:824–830
2. Camden JP, Dieringer JA, Zhao J, Van Duyne RP (2008) Controlled plasmonic nanostructures for surface-enhanced spectroscopy and sensing. Acc Chem Res 41(12):1653–1661
3. Gray SK (2007) Surface plasmon-enhanced spectroscopy and photochemistry. Plasmonics 2:143–146
4. Anker JN, Hall WP, Lyandres O, Shah NC, Zhao J, Van Duyne RP (2008) Biosensing with plasmonic nanosensors. Nat Mater 7:442–453
5. Mayer KM, Hafner JH (2011) Localized surface plasmon resonance sensors. Chem Rev 111(6):3828–3857
6. Atwater HA, Polman A (2010) Plasmonics for improved photovoltaic devices. Nat Mater 9:205–213
7. Green MA, Pillai S (2012) Harnessing plasmonics for solar cells. Nat Photon 6:130–132
8. Juan ML, Righini M, Quidant R (2011) Plasmon nano-optical tweezers. Nat Photon 5:349–356
9. Chen C, Juan ML, Li Y, Maes G, Borghs G, Van Dorpe P, Quidant R (2012) Enhanced optical trapping and arrangement of nano-objects in a plasmonic nanocavity. Nano Lett 12(1):125–132
10. Rang M, Jones AC, Zhou F, Li ZY, Wiley BJ, Xia Y, Raschke MB (2008) Optical near-field mapping of plasmonic nanoprisms. Nano Lett 8(10):3357–3363
11. Brioude A, Jiang XC, Pileni MP (2005) Optical properties of gold nanorods: DDA simulations supported by experiments. J Phys Chem B 109(27):13138–13142
12. Hicks EM, Zhang X, Zou S, Lyandres O, Spears KG, Schatz GC, Van Duyne RP (2005) Plasmonic properties of film over nanowell surfaces fabricated by nanosphere lithography. J Phys Chem B 109(47):22351–22358
13. Heo CJ, Kim SH, Jang SG, Lee SY, Yang SM (2009) Gold "nanograils" with tunable dipolar multiple plasmon resonances. Adv Mater 21(17):1726–1731
14. Aizpurua J, Hanarp P, Sutherland DS, Käll M, Bryant GW, García de Abajo FJ (2003) Optical properties of gold nanorings. Phys Rev Lett 90(5):057401
15. Hao F, Larsson EM, Ali TA, Sutherland DS, Nordlander P (2008) Shedding light on dark plasmons in gold nanorings. Chem Phys Lett 458(4–6):262–266
16. Nordlander P (2009) The ring: a leitmotif in plasmonics. ACS Nano 3(3):488–492
17. Larsson EM, Alegret J, Käll M, Sutherland DS (2007) Sensing characteristics of NIR localized surface plasmon resonances in gold nanorings for application as ultrasensitive biosensors. Nano Lett 7(5):1256–1263
18. Banaee MG, Crozier KB (2010) Gold nanorings as substrates for surface-enhanced Raman scattering. Opt Lett 35(5):760–762
19. Prodan E, Radloff C, Halas NJ, Nordlander P (2003) A hybridization model for the plasmon response of complex nanostructures. Science 302:419–422
20. Prodan E, Nordlander P (2004) Plasmon hybridization in spherical nanoparticles. J Chem Phys 120(11):5444–5454
21. Prodan E, Nordlander P (2003) Structural tunability of the plasmon resonances in metallic nanoshells. Nano Lett 3(4):543–547
22. Wang H, Wu Y, Lassiter B, Nehl C, Hafner JH, Nordlander P, Halas NJ (2006) Symmetry-breaking of individual plasmonic nanoparticles. Proc Natl Acad Sci USA 103(29):10856–10860
23. Radloff C, Halas NJ (2004) Plasmonic properties of concentric nanoshells. Nano Lett 4(7):1323–1327
24. Wang H, Brandl DW, Le F, Nordlander P, Halas NJ (2006) Nanorice: a hybrid plasmonic nanostructure. Nano Lett 6(4):827–832
25. Ye J, Van Dorpe P, Lagae L, Maes G, Borghs G (2009) Observation of plasmonic dipolar anti-bonding mode in silver nanoring structures. Nanotechnology 20(46):465203
26. Félidj N, Laurent G, Aubard J, Lévi G, Hohenau A, Krenn JR, Aussenegg FR (2005) Grating-induced plasmon mode in gold nanoparticle arrays. J Chem Phys 123(12):221103
27. Ye J, Chen C, Van Roy W, Van Dorpe P, Maes G, Borghs G (2008) The fabrication and optical property of silver nanoplates with different thicknesses. Nanotechnology 19(32):325702
28. Park TH, Mirin N, Lassiter JB, Nehl CL, Halas NJ, Nordlander P (2008) Optical properties of a nanosized hole in a thin metallic film. ACS Nano 2(1):25–32
29. Wu LY, Ross BM, Lee LP (2009) Optical properties of the crescent-shaped nanohole antenna. Nano Lett 9(5):1956–1961
30. Zou S, Janel N, Schatz GC (2004) Silver nanoparticle array structures that produce remarkably narrow plasmon lineshapes. J Chem Phys 120(23):10871–10875